China Ocean Engineering, Vol. 24, No. 2, pp. 353 - 368

Modelling Solitary Waves and Its Impact on Coastal Houses with SPH Method *

LIANG Dong-fang[a], N. I. Thusyanthan[b],
S. P. Gopal Madabhushi[a] and TANG Hong-wu (唐洪武)[c,1]

[a] *Department of Engineering, University of Cambridge, Cambridge CB2 1PZ, UK*
[b] *KW Ltd, Fetcham Park House, Lower Road, Fetcham, Surrey KT22 9HD, UK*
[c] *State Key Laboratory of Hydrology - Water Resources and Hydraulic Engineering, Hohai University, Nanjing* 210098, *China*

(Received 19 March 2009; received revised form 7 November 2009; accepted 22 January 2010)

ABSTRACT

The interaction between solid structures and free-surface flows is investigated in this study. A Smoothed Particle Hydrodynamics (SPH) model is used in the investigation and is verified against analytical solutions and experimental observations. The main aim is to examine the effectiveness of a tsunami-resistant house design by predicting the wave loads on it. To achieve this, the solitary wave generation and run-up are studied first. The solitary wave is generated by allowing a heavily weighted block to penetrate into a tank of water at one end, and the near-shore seabed is modelled by an inclined section with a constant slope. Then, the SPH model is applied to simulate the three-dimensional flows around different types of houses under the action of a solitary wave. It has been found that the tsunami-resistant house design reduces the impact force by a factor of three.

Key words: *solitary waves*; *tsunami*; *wave impact*; *coastal structures*; *SPH*

1. Introduction

Tsunamis and storm surges pose high threat to those living in coastal areas, e.g. the Boxing Day tsunami in South Asia, 2004 destroyed about 80000 houses and claimed around 300000 lives (Dia *et al.*, 2008). While tsunamis and storms are natural disasters that are unavoidable, it is possible to reduce their damage by building more resilient infrastructures. In the aftermath of the 2004 tsunami, a tsunami-resistant house project was developed at the SENSEable City Laboratory at Massachusetts Institute of Technology, in collaboration with Tsunami Design Initiative of Harvard Graduate School of Design and Buro Happold Engineers in London (TDI Design, 2005; Chen *et al.*, 2005). The design was presented to USAID in Washington DC in April 2005, and prototype houses were constructed by Prajnopaya Foundation and Sri Bodhiraja Foundation in September 2005. Thusyanthan *et al.* (2007) and Thusyanthan and Madabhushi (2008) carried out small-scale (1/25) tests in a tsunami wave tank and compared the performance of the traditional and tsunami-resistant houses under wave actions, but did not measure the wave loads on different parts of the house. Moreover, experimental study is often costly and time consuming. Therefore, a computer model, with the ability to deal with strong fluid/solid interactions and complex free-surface evolutions, can be a very useful tool to investigate tsunami

* This work was financially supported by the National Natural Science Foundation of China (Grant No. 50779014).
1 Corresponding author. E-mail: hwtang@hhu.edu.cn

wave loading on coastal structures. This paper presents such a numerical model, based on Smoothed Particle Hydrodynamics (SPH), to verify the structural design of the tsunami-resistant house.

Conventionally, the fluid motion is formulated in an Eulerian framework and the free surface positions are tracked with the facilitation of computational grids, as for the marker-and-cell (Harlow and Welch, 1965) and volume-of-fluid (Hirt and Nichols, 1981) methods. The Smoothed Particle Hydrodynamics (SPH) is a purely Lagrangian description of the fluid motion that does not rely on any grids (Lucy, 1977; Gingold and Monaghan, 1977), thus it offers new flexibility in handling the moving boundaries. The advantages of the SPH method include rigorous mass conservation, free of advection-related numerical diffusion and simplicity in programming. Early numerical experiments on the SPH method show that it gives fairly good results even with rather coarse resolutions (Monaghan, 1994). There have been an increasing number of applications of SPH method to a wide range of fluid dynamics problems. In connection with the current research topic, SPH model has been applied to wave run-up on a beach with cliffs (Monaghan and Kos, 1999), Scott Russell's wave maker (Monaghan and Kos, 2000), dam-break wave impact on a cylinder (Gómez-Gesteira and Dalrymple, 2004), underwater landslide (Ataie-Ashtiani and Shobeyri, 2008) and so on. Readers are referred to Monaghan (1992) for a general review, while Monaghan (1994) demonstrates a simple algorithm that extends SPH method to nearly-impressible flows.

Compared with laboratory experiments, numerical simulations provide an easier control on flow conditions and a wider scope on post analyses. While the dynamics of the solid blocks entering a fluid and the resulting solitary waves have been well studied by Monaghan *et al*. (2003), the present work focuses more on the impact of the generated waves on coastal houses of different designs. Before attempting the wave impact on houses, an in-house SPH model is validated in terms of wave generation, propagation and impact on a structure.

2. Numerical Method

2.1 Basic SPH Equations

In an SPH model, the water body is represented by lots of particles, which can be roughly regarded as small elements of fluid carrying a fixed mass and volume. These particles are actually interpolation points, with each associated with a velocity, pressure and density. The essence of the SPH method is the kernel interpolation technique, which allows a continuous function to be constructed from values on a set of disordered points. The Navier-Stokes equations can then be transformed into the following equations that govern the movement of each particle and the evolution of the fluid properties associated with it. This study adopts a standard SPH formulation for free surface flows.

$$\frac{\mathrm{d}\boldsymbol{v}}{\mathrm{d}t} = -\sum_j m_j\left(\frac{P_i}{\rho_i^2} + \frac{P_j}{\rho_j^2} + \Pi_{ij}\right)\nabla_i W_{ij} + \boldsymbol{g}; \tag{1}$$

$$\frac{\mathrm{d}\boldsymbol{r}_i}{\mathrm{d}t} = \bar{\boldsymbol{v}}_i = \boldsymbol{v}_i - \varepsilon\sum_j \frac{m_j}{\rho_i}(\boldsymbol{v}_i - \boldsymbol{v}_j)W_{ij}; \tag{2}$$

$$\frac{\mathrm{d}\rho_i}{\mathrm{d}t} = \sum_j m_j(\bar{\boldsymbol{v}}_i - \bar{\boldsymbol{v}}_j) \cdot \nabla_i W_{ij}; \tag{3}$$

$$P_i = C^2(\rho_i - \rho_0), \tag{4}$$

where t is time; i and j are particle indices; P, ρ, m, $\boldsymbol{v}$ and $\boldsymbol{r}$ denote the pressure, density, mass, velocity and position of a particle respectively; W_{ij} is short for the kernel function $W(\boldsymbol{r}_i - \boldsymbol{r}_j)$; $\nabla_i W_{ij}$ signifies the gradient of $W(\boldsymbol{r}_i - \boldsymbol{r}_j)$ with respect to the coordinates of particle i; $\boldsymbol{g}$ is the vector form of the gravitational acceleration with the vertical component being 9.8 m/s^2; ε is a constant specified to be 0.5 in this study; C is a user-specified sound speed taken to be 20 m/s herein; ρ_0 is the reference density set to 1000 kg/m^3; and the summations are over all the particles. In Eq. (1), Π_{ij} is the artificial viscosity term taking the form of:

$$\Pi_{ij} = -\frac{\alpha c h}{0.5(\rho_i + \rho_j)} \frac{\min(0, (\boldsymbol{v}_i - \boldsymbol{v}_j) \cdot (\boldsymbol{r}_i - \boldsymbol{r}_j))}{|\boldsymbol{r}_i - \boldsymbol{r}_j|^2 + 0.01h^2} \tag{5}$$

where h is the smoothing length scale set to 0.01 m for all the solitary wave cases and 0.005 m for the flood wave case, and α is a constant set to 0.001 for all the computations undertaken in this study. The interpolation kernel function, $W(\ )$, is an approximation of the Dirac delta function and should be differentiable. Here the cubic spline kernel function is used, which prescribes that one particle contributes to the movement of all its neighbouring particles within a radius of $2h$. The ordinary differential Eqs. (1) ~ (4) are integrated explicitly using a leapfrog time stepping scheme.

2.2 Solid Boundaries

Eqs. (1) ~ (4) describe the behaviour of the internal fluid particles only. Monaghan (1994) devises lines of virtual particles to resemble solid boundaries, which can be arranged into arbitrary shapes and can be either fixed or moved according to any specified rules in the course of the computation. To reduce the "roughness" of the wall represented by particles, the spacing of boundary particles is a half of the initial spacing between neighbouring fluid particles. Apart from the boundary particles, the SPH model developed in this study also admits the deployment of boundary equations, which specify the wall positions through algebraic equations and therefore significantly reduce the number of boundary particles needed (Liang, 2010). The boundary particles or walls interact with the flow by exerting a repulsive force on those fluid particles within a distance of r_0. If the distance between an inner particle i and a boundary k is found to be smaller than the threshold separation r_0, then the following term, having the units of force per mass, is added to the right hand side of Eq. (1).

$$\sum_k D\left[\left(\frac{r_0}{r_{ki}}\right)^4 - \left(\frac{r_0}{r_{ki}}\right)^2\right] \frac{\boldsymbol{n}_{ki}}{r_{ki}}, \tag{6}$$

where the summation is over all the boundaries, D is a problem dependent coefficient in an order of the square of the largest velocity, r_{ki} is the distance between the fluid particle i and the boundary particle or wall k, $\boldsymbol{n}_{ki}$ is the unit vector directed from the boundary k towards the fluid particle i. This formulation has been found to produce a repulsive force large enough to stop any penetration. Such a boundary treatment essentially enforces a slip boundary condition at walls.

2.3 Motion of the Solid Body

In the present study, the tsunami wave is generated by dropping a heavy weight into one end of the water tank. Simulating this process requires simultaneous solutions of the solid body motion and the fluid motion. At present, only the vertical movement of the rigid body is permissible, resembling the installation of vertical guide rails in the experiment to restrain motions in other directions (Monaghan and Kos, 2000). The falling velocity is determined according to Newton's second law.

$$M\frac{\mathrm{d}V}{\mathrm{d}t} = F, \tag{7}$$

where M is the mass of the rigid body, V is its falling velocity and F is the vertical force acting on the body which includes the gravity force, Mg, and the fluid reaction. The rigid body is represented by a set of boundary particles arranged into a desired shape. The flow-induced force on the rigid body can be calculated by summing up forces between the inner fluid particles and the relevant boundary particles:

$$-\sum_k \sum_i m_i D\left[\left(\frac{r_0}{r_{ki}}\right)^4 - \left(\frac{r_0}{r_{ki}}\right)^2\right]\frac{\boldsymbol{n}_{ki}}{r_{ki}}, \tag{8}$$

where the outer summation is over all the boundary particles constituting the rigid body and the inner summation is over all the fluid particles. Only the vertical component of the force is used in the present calculation.

At present, the interaction between the rigid body and flume walls is not considered. To avoid numerical difficulties, the movement of the rigid body is forced to stop if its distance to the tank bottom is smaller than two times the smoothing length ($2h$).

2.4 Simulation Procedure

For all the cases studied herein, the fluid particles are initially placed on a rectangular lattice with a constant interval of h, chopped by the boundaries. The smallest distance between the inner particles and the walls is r_0, so the initial repulsive force from the wall is zero. All particles are assigned the same initial density, ρ_0. Corresponding to the particles' relative motion, the density, and thus the pressure, changes as specified in Eqs. (3) and (4).

Before releasing the solid body, preliminary simulations are conducted to attain a hydrostatic pressure distribution within the confined water body. To accelerate the dissipation of fluid kinetic energy, which arises because the initial pressure field and gravity force are unbalanced, a large artificial viscosity is imposed. Once the static equilibrium state is achieved and the rigid body is activated, the artificial viscosity is reset to the normal value.

3. Solitary Wave Generation

The falling of a rectangular block into a tank of water is described in this section. In the computation, the tank is 3 m long, 0.4 m wide and infinitely high, with the bottom being horizontal and sidewalls vertical. The water depth is 0.21 m. A rectangular block, having a length of 0.3 m, width of 0.4 m, height of 0.4 m and mass of 38.2 kg, is located with its bottom face in contact with the water

surface initially. Then, the solid block is released and descends into the tank under its own weight, inducing a solitary wave travelling to the other end of the tank. This wave generator is the same, in principle, as that used by Scott-Russell in his classic demonstration of solitary wave formation, which has been studied using SPH by Monaghan and Kos (2000) and Ataie-Ashtiani and Shobeyri (2008).

The shape of the water body can be conveniently visualised by drawing the scatter plot of smoothed particles, as seen in Fig. 1. Some of the snapshots are taken at the same time as those shown in Monaghan and Kos (2000) and Ataie-Ashtiani and Shobeyri (2008) for comparison purposes. As the block enters water, the fluid immediately underneath is pushed downward, whereas a vigorous jet of water is heaved up from the bottom-right corner of the block. The jet overturns and strikes on the surface of the block, while the water surface remains calm further away from the block, see Fig. 1a. Apart from a downward moving component, the underneath particles also exhibit a strong rightward moving behaviour, as the water under the block is rapidly squeezed out. However, the water that has been heaved up cannot move to the right as fast, so the water jet overturns forming a vortex that rotates anticlockwise as shown in Figs. 1b and 1c. Fig. 1d shows that the hollow vortex collapses as it moves away from the block and generates a small surge rising up against the right face of the block. In the meantime, a large wave emerges and travels down the tank. As this wave propagates rightward, small-scale distortions at the free surface dissipate and the free surface rapidly adjusts its shape into the solitary wave profile. For classical Kortweg de Vries solitary waves, the water surface level satisfies the following equation.

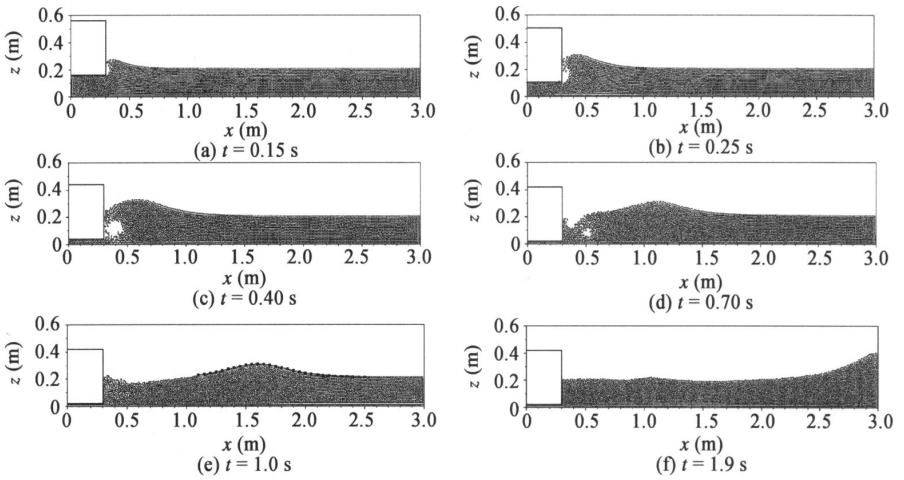

Fig. 1. Solitary wave generation with block mass of 38.2 kg.

$$\eta(x,t) = d + A\mathrm{sech}^2\left[\sqrt{\frac{3A}{4d^3}}(x - ct)\right], \tag{9}$$

where x is the axis along which the wave propagates, A is the wave amplitude, d is water depth, and the wave celerity c is given by

$$c = \sqrt{g(d + A)}, \tag{10}$$

The analytical water surface profile, with $ct = 1.6$ m and $A = 0.1$ m, is plotted in Fig. 1e as the solid line interspersed with large square symbols, which shows a good match with the simulated results. In Fig. 1f, the wave is reflected back after hitting the right-end wall, and the turmoil in the vicinity of the block has almost subsided. Qualitative examination of these snapshots shows good agreements with the previous simulations, although the results of Monaghan and Kos (2000) and Ataie-Ashtiani and Shobeyri (2008) are not shown here due to the page limit.

Through dimensional analysis, supported by experimental data, Monaghan and Kos (2000) obtained the following general expression for the normalised sinking velocity of the block.

$$\frac{V}{\sqrt{gd}} = \sqrt{\frac{M}{\rho_0 L^2 W}} \frac{Z}{d} \sqrt{1 - \frac{Z}{d}}, \tag{11}$$

where L is the length of the box, W is the width of the box, and Z is the thickness of the water layer beneath the block. Z can be easily converted into the displacement of the rigid block. As shown in Fig. 2, the falling speed increases rapidly at the early stage of the sinking (with large Z/d), and gradually slows down later on. The simulated falling speed experiences some oscillations, but fits reasonably well to the analytical curve. Given the crude assumptions used in deriving the analytical formula, the agreement between this scaling relation and the simulation results is satisfactory. The dynamic interaction between the sinking block and water is correctly captured.

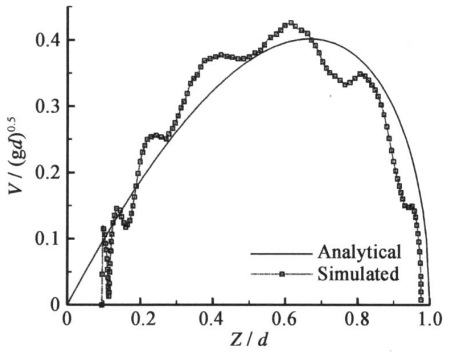

Fig. 2. Variation of the falling velocity of the block (Mass = 38.2 kg).

By assuming that a fixed percentage of gravitational energy of the falling block turns into the energy of the solitary wave, Monaghan and Kos (2000) established the relationship between the wave amplitude and the block mass, M, as follows.

$$\frac{A}{d} = 3\left(\frac{M}{40\rho L d W}\right)^{2/3}\left(\frac{L}{d}\right)^{2/3}. \tag{12}$$

The simulations are repeated for a range of block weights, with the generated wave heights listed in Table 1. The analytical and simulated wave heights agree well for lighter weights, which generate smaller waves, but show a large discrepancy for heavier blocks, which generate larger waves. For larger waves, the aforementioned solitary wave theory breaks down, as the wave amplitude can no longer

be deemed as sufficiently small. As can be seen in Fig. 3, the profile of a large wave contains a very sharp crest and is asymmetrical.

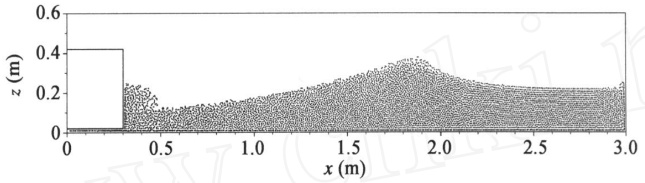

Fig. 3. Water surface profile at $t = 1.0$ s with block mass of 70 kg.

4. Solitary Wave Run-up

The setup of this scenario is similar to that in the previous section, but the end wall on the right is now replaced by a ramp and an elevated flat section backed by a vertical end-wall. The intention is to mimic the narrow coastal plains bounded by the ocean and steep cliffs. Adopting this setup, experiments were performed by Monaghan and Kos (1999). The main dimensions are kept the same as those in the experiment, e.g. 0.4 m wide tank and 0.21 m high ramp with a horizontal length of 0.98 m, 0.52 m long flat section on the right. The initial water depth is 0.21 m, hence the ramp is totally under water and the flat section on the right is initially dry. In order to reproduce the experimental wave height of 0.088 m, a 35 kg block is used in the computation, as suggested in Table 1.

Table 1 Amplitudes of the solitary wave generated by blocks of different weights

M (kg)	A/d (Analytical)	A/d (Simulated)
30.0	0.37	0.38
38.2	0.44	0.48
50.0	0.52	0.60
60.0	0.59	0.70
70.0	0.65	0.79

Fig. 4 shows the snapshots of the water surface position and compares the SPH predictions with the experimental photographs at corresponding instants, which clearly illustrate how the solitary wave is transformed by the topography. As the wave moves into the shallower depths, it steepens and becomes asymmetrical as shown in Fig. 4a. As the wave travels across the ramp and spills onto the dry horizontal plain, no breakage occurs. Fig. 4b shows the time when the solitary wave has just touched the vertical wall. Later on, water impinges against the vertical wall and rises up, producing splashes in the upper part of the ascending jet, as seen in Fig. 4c. After reaching its highest position, the flow front curls back and plunges into the underneath fluid. Although the plunging wave is now heading backward, the underlying fluid still advances forward. Thus highly disturbed flow is produced near the right wall at subsequent times, as evidenced by the highly irregular perturbations observed in the predicted

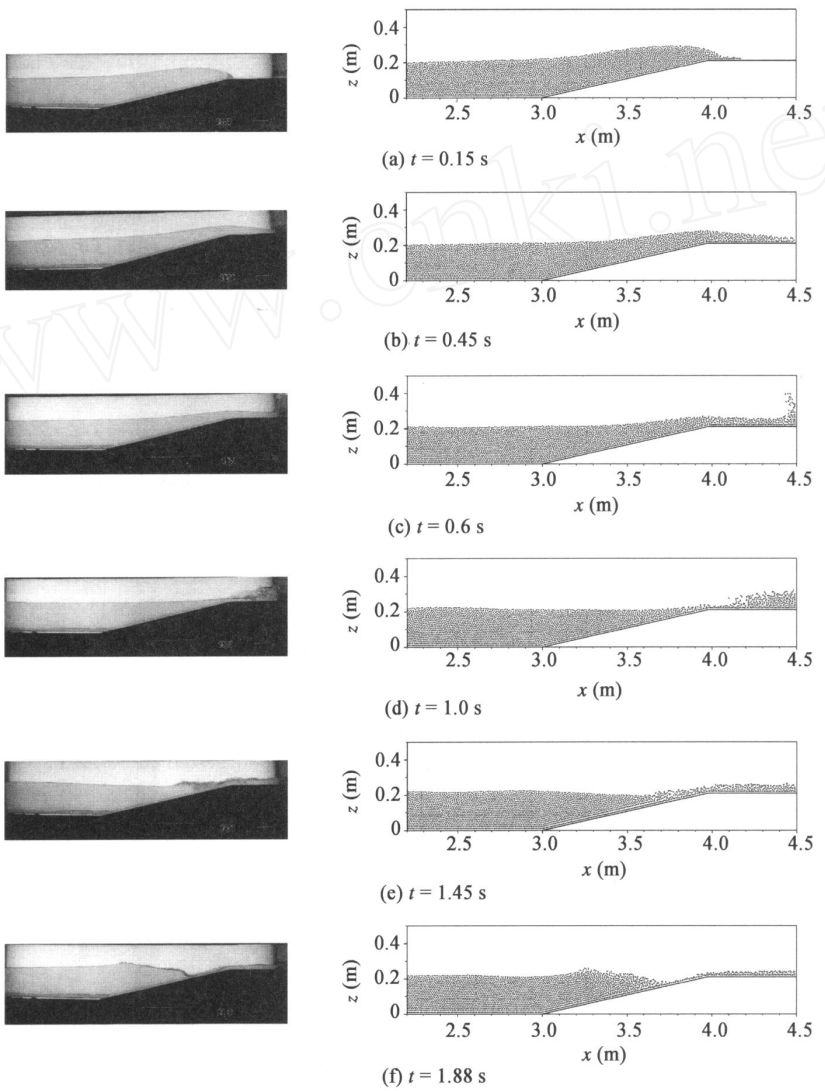

Fig. 4. Snapshots of solitary wave run-up: left-experimental photographs, right-SPH simulations.

free surface in Fig. 4d. Accompanying the high velocity and strong turbulence is the large water depth, deeper than that occurred in the first strike of the solitary wave on the horizontal plain. A comparison between Figs. 4b and 4d indicates that the return wave will cause more destruction than the run-up of a storm surge or tsunami wave, as also rightly inferred by Monaghan and Kos (1999). Eventually, the backflow becomes dominant and a thin layer of water moves left and runs down the slope, which can be seen in Figs. 4e ~ 4f. In Fig. 4f, a small dip is created on the upper half of the slope where the shallow stream enters the deeper water. Another consequence of the return flow is that it

pushes the surface water to the left and induces a small bore wave to the left of the dip. Fig. 4 shows that the bulk features of the entire flow process are well reproduced. The consistent agreement in the surface shapes throughout the wave transformations suggests that the SPH model correctly captures the physics of the flow.

5. Flood Wave Impact on An Idealised Structure

Owing to the nature of the Lagrangian approach, the SPH simulations often suffer from spurious pressure oscillations, although the velocity field and water surface position can be predicted satisfactorily. Because the impact force is the integration of pressure over an area, most of spurious oscillations in the pressure field can be filtered out through the integration process. Therefore it is possible that SPH predictions provide a credible estimation on the forces experienced by structures. One illustration can be found in Section 3, where a good agreement is achieved between the simulated and analytical falling velocity of the block (Fig. 2). Since this falling velocity is dependent on the force acting on the block, it reveals that the fluid force must have been predicted correctly. Another illustration is given below.

The interaction of a flood wave with an idealised structure has been studied by means of physical modelling by Professors Catherine Petroff and Harry Yeh of the University of Washington, Seattle. Their work has been used by Gómez-Gesteira and Dalrymple (2004) in SPH simulations. The experimental setup mainly consists of a rectangular flume and a prismatic structure. The flume is enclosed with a length of 1.6 m and a width of 0.61 m. The cross section of the structure is square with a side length of 0.12 m. The flume sidewalls are tall enough to confine flows within the flume. The structure is also tall enough to avoid being overtopped. Taking a bottom corner of the flume as the origin of the coordinates with x and y axes along the longer and shorter sidewalls of the flume respectively, the structure stands on the flume bed with $x = 0.9 \sim 1.02$ m and $y = 0.25 \sim 0.37$ m. Initially a very thin plate divides the flume into two compartments at $x = 0.4$ m. The compartment that does not contain the structure is filled with water to a depth of 0.3 m, while the other compartment is submerged by an approximately 0.01 m deep water layer at the beginning of the experiment. Initially the water is at rest. By swiftly removing the thin plate, water is released to impact on the structure. In the present simulation, the smoothing length used is 0.005 m.

Fig. 5 demonstrates the flow evolution via a series of water surface plots. The flood front has just arrived at the front face in Fig. 5a at $t = 0.3$ s. After the flood wave impinges on the structure, a reflection wave is generated. At the same time, the flood wave keeps progressing downstream and wraps around the structure from the two sides, see Fig. 5b. Once the two diffractive waves collide with each other behind the structure, as shown in Fig. 5c, a local peak in the water level arises. Fig. 5c also shows the moment when the flood front is about to reach the right end wall of the flume. As seen in Fig. 5d, the free surface undergoes severe deformation after the flood front hits the end wall.

The time histories of the net x-component force acting on the structure and the x-component velocity at point ($x = 0.754$ m, $y = 0.31$ m, $z = 0.026$ m) are compared with the values collected in

the experiment, as shown in Fig. 6. Generally, the SPH model provides a favourable agreement with the measurements. The present SPH model gives an even better agreement with the measurements than the SPH model in Gómez-Gesteira and Dalrymple (2004), which may be attributed to the higher resolution.

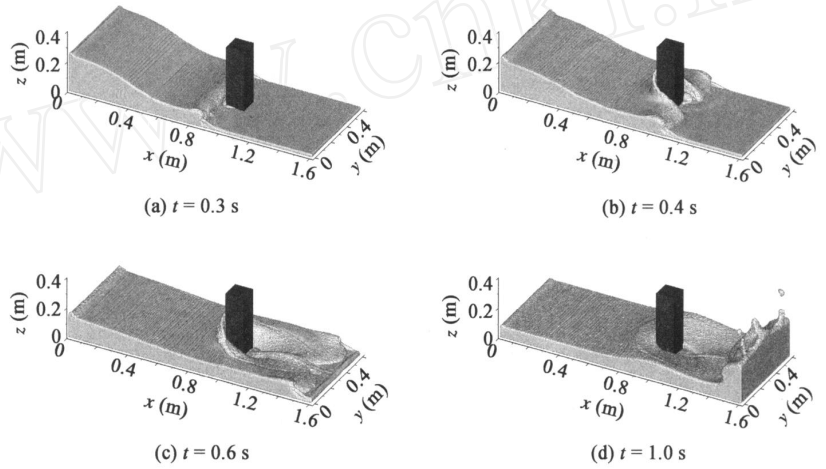

Fig. 5. Water surface positions for the wave/structure interaction problem.

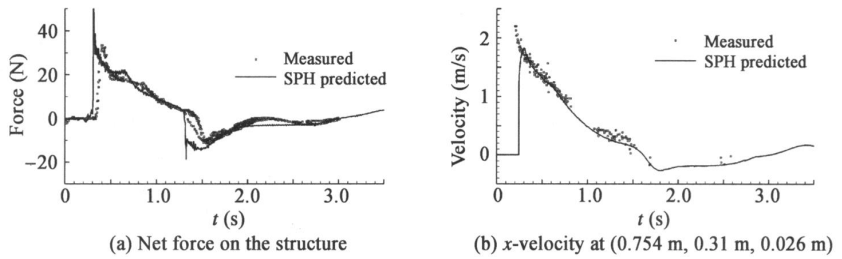

Fig. 6. Comparisons of the measured and predicted data for the wave/structure interaction problem.

6. Solitary Wave Impact on Coastal Houses

By the SPH model, wave loads on coastal houses are predicted, and thus the effectiveness of the tsunami-resistant house design is verified. The main idea of the more resilient design, proposed by TDI Design (2005) and Chen *et al*. (2005), is to actively allow the passage of water. Instead of a continuous wall with small doors and windows that encloses an internal space in the traditional design as shown in Fig. 7a, the new design leaves a big opening in the middle section of the end walls parallel to the shoreline. The opening is covered with louvered panels made of bamboo or wood, as seen in Figs. 7b and 7c. Therefore, the middle section of the end walls is porous, and is relatively weak so as

to be easily pushed open by high-speed flows. The openings in the end walls, together with doors in the side walls, break the outer wall up into four independent parts. The roof of the tsunami-resistant house thus sits on these four core columns, each at one corner. Such a design requires less bricks and concrete in the construction. The bamboo and wood are materials that can be easily found locally and are environmentally friendly. More importantly, four independent short walls can withstand a larger lateral force imposed by water pressure than a single continuous wall. Besides, porous walls provide less intrusion to the flow and thus attract less hydrodynamic loads. Apart from the opening at end walls, the base floor of the house is raised above the ground in the design as shown in Fig. 7b, thus leaving an extra path for the water to flow underneath. This tsunami-resistant design has been implemented in Balapitiya in Sri Lanka in September 2005, and Fig. 7c shows a prototype house built after adopting the above concept. In practice, the essential features are retained, but modifications to the original design have to be made to suit with the local culture, climate, and tradition, i.e. the gap beneath the floor is scrapped in Fig. 7c due to the fear of snakes hiding underneath.

(a) Traditional houre in Sri Lanka

(b) Tsunami-resistant house design

(c) Tsunami-resistant house built in Sri Lanka

(d) Tsunami-resistant house in computation

Fig. 7. Coastal houses.

A 1/25 scale model of the tsunami-resistant house, as shown in Fig. 7d, is tested. Important dimensions are listed in Table 2. The coastal region in South Asia is usually composed of beaches and plains with gentle slopes rather than cliffs, so the right boundary of the computational domain is open. The geometry of the domain is similar to the laboratory experiments described in Thusyanthan *et al.* (2007), Modoni (2007) and Thusyanthan and Madabhushi (2008). In this three-dimensional simulation, the water tank was shortened by discarding the left 2 m of tank to reduce computational cost. Thus, the block, used to initiate a large wave, now resides at $x = 2 \sim 2.3$ m, and has a mass of 38.2 kg. The house is placed on the shore with its base occupying a region with $x = 4.05 \sim 4.41$ m along the centreline. The shoreline is initially 0.02 m below the house. Fig. 8 shows the instant when the

block is entering the water, thereby the reversed plunging wave adjacent to the block can be clearly seen.

Table 2 Key dimensions of the tsunami-resistant house model

Base floor area	0.36 m × 0.20 m
Cross section	0.30 m × 0.20 m
Horizontal projected area of roof	0.36 m × 0.20 m
Height from base floor to roof top	0.15 m
Gap between base floor and ground	0.02 m
Slope of the roof	24°
Width of the door in side walls	0.05 m
Width of the opening in end walls	0.11 m

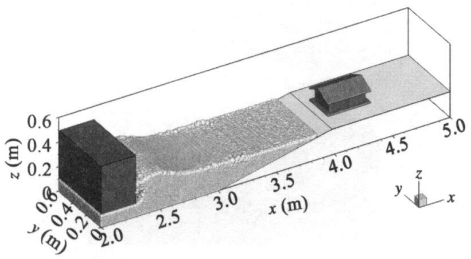

Fig. 8. Configuration of the computation: traditional house design, $t = 0.3$ s.

Fig. 9 illustrates a sequence of side views of the impact process between the run-up wave and coastal houses. Three house designs are considered: without either the end opening or the raised floor, with both the end opening and the raised floor, and with the end opening but without the raised floor. They are referred to as traditional design, original tsunami-resistant design and modified tsunami-resistant design respectively in the following. As the wave hits the house of traditional design, water curls up and splashes backwards, whereas the other two houses produce much less splash. The house of tsunami-resistant design generates the least splash, and Fig. 9 also clearly reveals that some amount of water passes through the gap between the raised floor and the ground. The space inside the house behaves like a cushion, which is effectively activated by creating the end openings. As the incoming water hits the front wall, some enters the house through the front opening. After the wave front passes, water inside the house rushes out through the rear opening and also, to a less extent, via the side doors, as can be noticed by close examination of Fig. 9e.

Forces experienced by different parts of the house are monitored in the simulation. The horizontal force on the front wall and the uplift force on the roof are two most important forces that determine the structural stability, so they are plotted in Fig. 10. It is found that the water front approaches houses at a speed of about 1.0 m/s and with a depth of about 0.08 m. The maximum horizontal force on the front wall can be estimated by applying the momentum equation to a control volume in front of the house. Taking the house of traditional design for example, the hydrostatic force acting on a vertical

plane some distance upstream of the house, which is parallel to and of the same width as the house front wall, is

$$\frac{1000 \times 9.8 \times 0.08}{2} \times (0.2 \times 0.08) \approx 6.3 \text{ N}$$

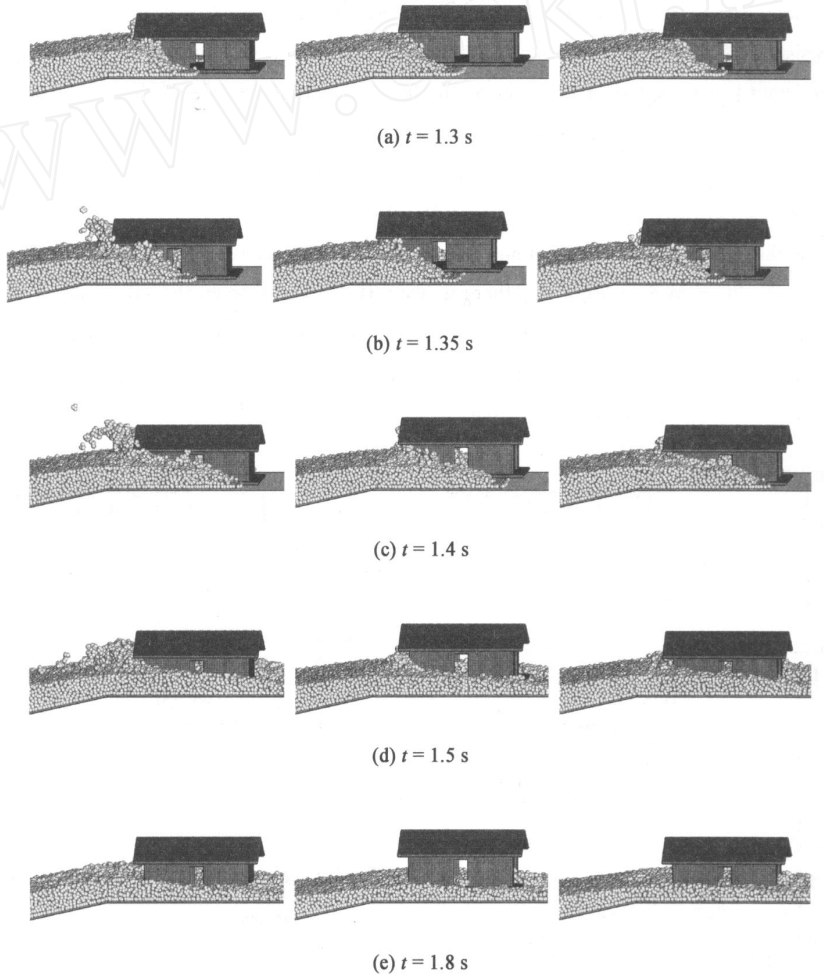

Fig. 9. Wave/house interaction: left – traditional design, middle – original tsunami-resistant design, right – modified tsunami-resistant design.

The momentum flux across this vertical plane is

$$1000 \times 1.0 \times (0.2 \times 0.08) = 16.0 \text{ N}$$

Assuming that the horizontal momentum flux immediately in front of the house is zero, then the summation of the above two numbers, 22.3 N, equals the horizontal force acting on the front wall. Bearing in mind the unsteadiness and three-dimensionality of the flow, this crude analysis underestimates the peak

force plotted in Fig. 10a by about 10 N. This underestimation is expected, since the momentum flux immediately in front of the house is not actually zero. The flow curls back after hitting the front wall and thus possesses a momentum opposite to the incoming flow, resulting in a larger change of momentum flux and thus a larger impact force on the house. For modified tsunami-resistant design, forces on the front wall and roof are both reduced to about one third of the values for the traditional design, although its front area is only reduced by a half. It implies that the impact pressure on the surface of the tsunami-resistant house is lower than that of the traditional house. As expected, forces on the original tsunami-resistant house are the smallest among the three, especially for the lift force on the roof, since it not only has openings at end walls but also is located 0.02 m higher than the other two houses. As seen from Fig. 9, a thin water layer at the wave front can pass through the gap between the elevated base floor and the ground, without making contact with the front wall. This explains the delayed and steep rise of the impact force on the front wall of original tsunami-resistant house as shown in Fig. 10b. For all the three cases in Fig. 10, there is about 0.1 s lag between the inflictions of the lift and horizontal forces, which corresponds the time taken for water to climb up the front wall. Despite this time lag, the peak values of the horizontal and vertical forces almost concur, except for the original tsunami-resistant house which experiences only a very small vertical force.

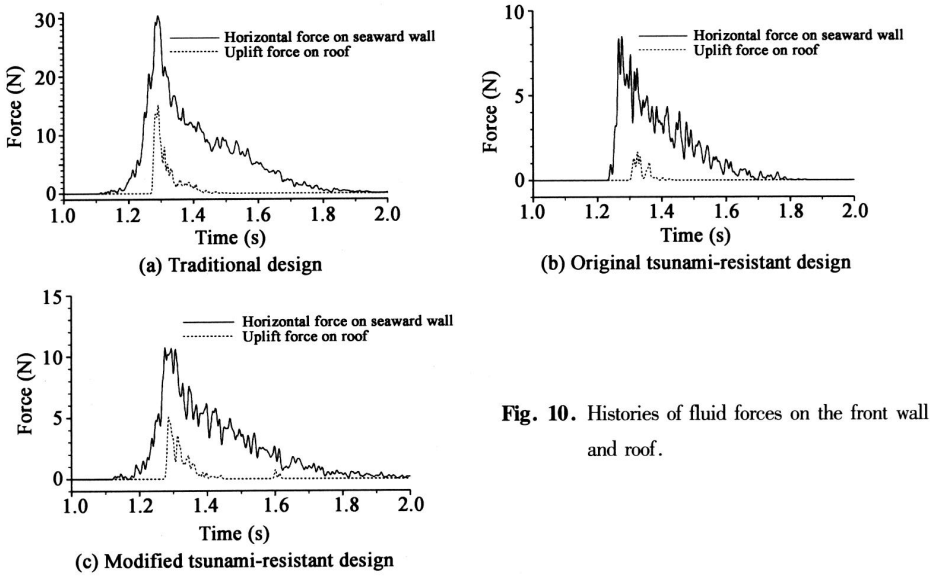

Fig. 10. Histories of fluid forces on the front wall and roof.

If the Froude number is assumed to be the same between the model and the prototype, then the ratio of the model velocity to the prototype velocity is the square root of the length scale, which is $(1/25)^{0.5} = 1/5$. Consequently, the pressure felt by the model houses is 1/25 of that by the prototype houses. As being noted that the force is proportional to pressure multiplied by area, it suggests that the impact force at full scale can be expected to be 15625 times larger than the values mentioned in the previous paragraph.

The findings herein are consistent with the observation in the laboratory experiments that the traditional house model suffered severe damage and its roof is lifted off by the high-speed flow, while the tsunami-resistant house is free of any damage (Thusyanthan *et al.*, 2007; Thusyanthan and Madabhushi, 2008). By keeping the house standing upon the impact, lives can be saved, and a good starting point is provided for people to recover after the disaster.

7. Conclusions

An SPH model has been developed and used to study the behaviour of the coastal houses subject to the impact of a solitary wave, which may occur in a tsunami or a storm surge. The near-shore wave condition is created by dropping a heavy solid block at one end of the water tank. The highly distorted free surface and complex interaction at fluid/solid boundary are modelled. The SPH method has been demonstrated to be very promising for these moving boundary problems.

The first case presented is the generation of solitary waves and the simulation is validated using data in Monaghan and Kos (2000). As the block makes its way towards the bottom, it drives water to form a reversed plunging wave and a solitary wave. While the reversed plunging wave collapses and dissipates its energy in the region very close to the block, the solitary wave propagates towards the other end of the tank. The motion of the rigid block, the form and speed of the solitary wave are in good agreements with theory. The second case studied is a solitary wave travelling over a slope and then onto a coastal plain backed by a vertical wall. The simulated water surface shapes compare favourably with those observed in the experiment of Monaghan and Kos (1999). These two applications have implications on the waves induced by landslides and avalanches along banks. The third application shows that the SPH model can predict the impact force on structures correctly. The last application examines the design principle of tsunami-resistant houses. It has been found that even without being elevated, the forces on the front wall and the roof are reduced by about three times. The smaller impact force on the front wall can be explained by the reduced impact pressure and projection area, while the reduced lift force on the roof can be attributed to the enlarged flow passage and thus weakened vertical run-up. More reduction can be achieved, especially in terms of the lift force, if the gap beneath the base floor is retained. These findings are in line with those made from laboratory experiments. Therefore, the structural design of the tsunami-resistant house is proved to be effective.

References

Ataie-Ashtiani, B. and Shobeyri, G., 2008. Numerical simulation of landslide impulsive waves by incompressible smoothed particle hydrodynamics, *Int. J. Numer. Methods fluids*, **56**(2): 209 ~ 232.

Chen, E., Ho, E., Jallad, N., Lam, R., Lee, J., Zhou, Y., Del, Re D., Berrios, L., Nicolino, W. and Ratti, C., 2005. Resettlement or resilience? The tsunami safe(r) project, *Proceedings of the International Symposium on Disaster Reduction on Coasts*, Melbourne, Australia, 1 ~ 11.

Dias, P., Dissanayake, R. and Chandratilake, R., 2008. Lessens learned from tsunami damage in Sri Lanka, *Proceedings of ICE – Civil Engineering*, **159**(2): 74 ~ 81.

Gingold, R. A. and Monaghan, J. J., 1977. Smoothed particle hydrodynamics: theory and application to non-spherical

stars, *Monthly Notices of the Royal Astronomical Society*, **181**, 375 ~ 389.

Gómez-Gesteira, M. and Dalrymple, R. A., 2004. Using a three-dimensional smoothed particle hydrodynamics method for wave impact on a tall structure, *J. Waterw. Port Coast. Ocean Eng.*, **130**(2): 63 ~ 69.

Harlow, F. H. and Welch, J. E., 1965. Numerical calculation of time-dependent viscous incompressible flow of fluid with a free surface, *Phys. Fluids*, **8**(12): 2182 ~ 2189.

Hirt, C. W. and Nichols, B. D., 1981. Volume of fluid (VOF) method for the dynamics of free boundaries, *J. Comput. Phys.*, **39**(1): 201 ~ 225.

Liang, D., 2010. Evaluating shallow water assumptions in dam-break flows, *Proceedings of the Institution of Civil Engineers-Water Management*, **163**(5): 227 ~ 237.

Lucy, L. B., 1977. A numerical approach to the testing of the fission hypothesis, *The Astronomical Journal*, **82**, 1013 ~ 1024.

Modoni, A., 2007. *Tsunami resistant structures*, MEng thesis, Department of Engineering, University of Cambridge.

Monaghan, J. J., 1992. Smoothed particle hydrodynamics, *Annual Review of Astronomy and Astrophysics*, **30**, 543 ~ 574.

Monaghan, J. J., 1994. Simulating free surface flows with SPH, *J. Comput. Phys.*, **110**(2): 399 ~ 406.

Monaghan, J. J. and Kos, A., 1999. Solitary waves on a Cretan beach, *J. Waterw. Port Coast. Ocean Eng.*, **125**(3): 145 ~ 154.

Monaghan, J. J. and Kos, A., 2000. Scott Russell's wave generator, *Physics of Fluids*, **12**(3): 622 ~ 630.

Monaghan, J. J., Kos, A. and Issa, N., 2003. Fluid motion generated by impact, *J. Waterw. Port Coast. Ocean Eng.*, **129**(6): 250 ~ 259.

Thusyanthan, N. I. and Madabhushi, S. P. G., 2008. Tsunami wave loading on coastal houses: a model approach, *Proceedings of ICE – Civil Engineering*, **161**(2): 77 ~ 86.

Thusyanthan, N. I., Modoni, A., Hakin, R. and Madabhushi, S. P. G., 2007. Model study of tsunami wave loading on coastal structures, *Proceedings of the First Sri Lanka Geotechnical Society International Conference on Soil and Rock Engineering*. Colombo, 5 ~ 11.

TDI Design, 2005. Tsunami safer house design for the Prajnopaya Foundation, http://senseable.mit.edu/tsunami-prajnopaya/